Effect of Pulsed Current on Charging Performance of Lithium-ion Batteries

Huang, Xinrong; Liu, Wenjie; Acharya, Anirudh Budnar; Meng, Jinhao; Teodorescu, Remus; Stroe, Daniel-Ioan

Published in:
IEEE Transactions on Industrial Electronics

DOI (link to publication from Publisher):
10.1109/TIE.2021.3121726

Publication date:
2022

Document Version
Accepted author manuscript, peer reviewed version

Citation for published version (APA):
Huang, X., Liu, W., Acharya, A. B., Meng, J., Teodorescu, R., & Stroe, D.-I. (2022). Effect of Pulsed Current on Charging Performance of Lithium-ion Batteries. *IEEE Transactions on Industrial Electronics*, *69*(10), 10144-10153. https://doi.org/10.1109/TIE.2021.3121726

Effect of Pulsed Current on Charging Performance of Lithium-ion Batteries

Xinrong Huang, *Student Member, IEEE*, Wenjie Liu, *Student Member, IEEE*, Anirudh Budnar Acharya, Jinhao Meng, *Member, IEEE*, Remus Teodorescu, *Fellow, IEEE*, and Daniel-Ioan Stroe, *Member, IEEE*

***Abstract*—The pulsed current has been proposed as a promising battery charging technique to improve the charging performance and maximize the lifetime for Lithium-ion (Li-ion) batteries. However, the effect of the pulsed current charging is inconclusive due to the changeable current mode and conditions. This paper systematically investigates the effect of various pulsed current charging modes, i.e., Positive Pulsed Current (PPC) mode, Pulsed Current-Constant Current (PCCC) mode, Negative Pulsed Current (NPC) mode, Alternating Pulsed Current (APC) mode, Sinusoidal-Ripple Current (SRC) mode, and Alternating Sinusoidal-Ripple Current (ASRC) mode on battery performance. Moreover, a comprehensive analysis of the frequency impact on the quality of the current mode is performed. The current modes in this work are evaluated considering the maximum rising temperature, discharging capacity, and charging speed according to experimental results. Furthermore, this work provides guidance for developing pulsed current charging strategies to satisfy future charging requirements.**

***Index Terms*—Lithium-ion battery, pulsed current, sinusoidal-ripple current, charging performance**

I. INTRODUCTION

THE last decade has witnessed the booming popularity of electric vehicles (EVs) [1]. With the strong support of the governmental incentives worldwide, the annual sales of EVs have increased from 2 to 753 thousand [2]. Lithium-ion (Li-ion) batteries stand out among numerous commercial batteries applied in EVs due to their high energy and power density, long lifetime, and low self-discharge rate [3]. However, unlike traditional internal combustion engines that can quickly replenish fuel, EVs require a relatively long time to fully charge the batteries [4]. Therefore, fast charging capability is one of the bottlenecks faced by Li-ion batteries in EVs. Fast charging can be implemented by a high current rate to reduce the charging time. However, besides reducing the available discharging capacity, the high current rate will cause an increase in the battery temperature, which results in capacity degradation and a decrease in battery service life [5]. The Constant Current-Constant Voltage (CC-CV) mode is the standard method for charging Li-ion batteries [6], [7]. According to the capacity measurement in [8], the CV phase accounts for 48% of the entire charging time of the CC-CV mode, while it provides only 22% of the discharging capacity. Thus, the owner of the fast charging stations recommends to the users not charging the battery using the CV phase, which is leading to double charging time in EV applications [9]; however, this will reduce the available discharging capacity for batteries. Therefore, achieving a tradeoff between the charging speed, discharging capacity, and lifetime has been a significant target of numerous studies to develop an advanced charging strategy.

Pulsed current charging has been proposed to improve the charging performance and extend the battery lifetime [10]–[12]. However, other studies claim that the pulsed current charging has a negative impact on the charging performance and lifetime of Li-ion batteries [8], [13]. Moreover, the difference in the current parameters, e.g., frequency, amplitude, and current direction, could also cause opposite effects on the battery performance [14], [15]. The sinusoidal-ripple current charging is often mentioned and compared with pulsed current charging and its effect on Li-ion batteries is also inconclusive [8], [16], [17]. Most previous works investigate the effect of only one or two current charging modes on the battery performance and compare these to CC or CC-CV charging. This paper is the first work that considers all existing pulsed current modes and sinusoidal-ripple current modes and compares their performance through experimental tests.

The objective of this work is to systematically investigate and analyze the effect of the pulsed current charging and sinusoidal-ripple current charging on battery performance in terms of the maximum rising temperature, discharging capacity, and charging speed. Section II summarizes the existing research on these two charging methods, including six current modes, as shown in Fig. 1. The evaluation criteria for the charging performance investigated in this work are introduced in Section III. The experimental results and analysis are presented in Section IV. The conclusions are given in Section V.

II. BACKGROUND ON PULSED CURRENT CHARGING

A. Positive Pulsed Current (PPC) Mode

The Positive Pulsed Current (PPC) mode is the constant current charging with periodic relaxation time, as shown in Fig. 1(a) [18]. The period of the pulsed current is T, while

This work was supported in part by the China Scholarship Council under grant CSC201806290017, in part by European Union's Horizon 2020 research and innovation programme under the Marie Skłodowska-Curie grant agreement 845122, in part by Sichuan Science and Technology Program under grant 2021YJ0063, and in part by the National Natural Science Foundation of China under grant 52107229. (Corresponding author: W. Liu.)

X. Huang, W. Liu, A. B. Acharya, R. Teodorescu, and D. Stroe are with the Department of AAU Energy, Aalborg University, Aalborg 9220, Denmark (e-mails: hxi@et.aau.dk, wie@et.aau.dk, abac@et.aau.dk, ret@et.aau.dk, dis@et.aau.dk).

J. Meng is with the College of Electric Engineering, Sichuan University, Chengdu 610065, China (e-mail: jinhao@scu.edu.cn).

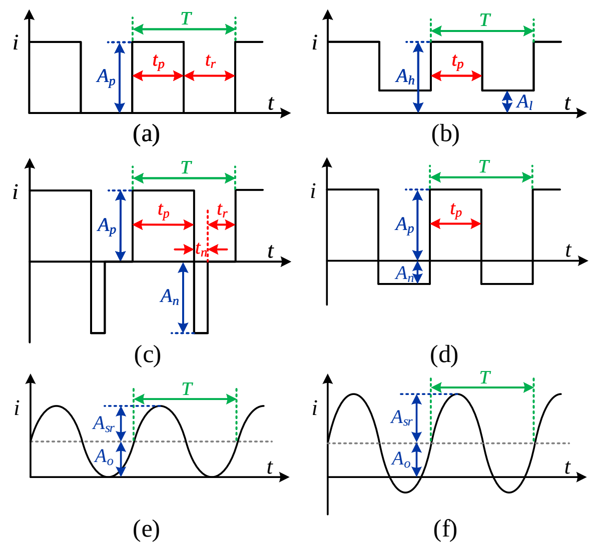

Fig. 1. Current modes: (a) Positive Pulsed Current (PPC) mode, (b) Pulsed Current-Constant Current (PCCC) mode, (c) Negative Pulsed Current (NPC) mode, (d) Alternating Pulsed Current (APC) mode, (e) Sinusoidal-Ripple Current (SRC) mode, and (f) Alternating Sinusoidal-Ripple Current (ASRC) mode.

the frequency f is $1/T$. The amplitude of the positive pulses is A_p. The duration of the positive pulsed current and of the relaxation period are t_p and t_r, respectively. Then, the duty cycle D_p of the PPC mode is defined as follows:

$$D_p = \frac{t_p}{T} \tag{1}$$

In [16], the PPC mode at the frequency, which returns the minimum impedance f_{Zmin} (around 1 kHz) can increase the discharging capacity and reduce the charging time by 2.1% and 16.8%, respectively. This frequency can be obtained by Electrochemical Impedance Spectroscopy (EIS) test. In [8], Positive Pulsed Current-Constant Voltage (PPC-CV) mode at f_{Zmin}, i.e., 2 kHz, can reduce the charging time by 0.6%, while the discharging capacity can be improved by 0.2%, compared with the CC-CV mode. Considering only the PPC phase of the PPC-CV mode, the charging time and the charging capacity are reduced by 47.2% and 20.8% compared with the CC-CV mode. This conclusion is different from that in [16], which indicates that the PPC mode without the CV phase can obtain a higher capacity compared to the CC-CV mode. Furthermore, compared to the CC-CV mode, the maximum rising temperature is increased by 52% in [8], while it is decreased by 36.4% in [16]. In [17], the PPC mode has no impact on the charging time but results in an increased cell temperature compared with the CC mode. In [15], the PPC-CV mode at a frequency of 1 kHz has no significant impact on battery lifetime but can reduce the charging time by 17%, while it at 50 Hz and 100 Hz can result in a faster capacity fade compared with the CC-CV mode during the cycling [15]. In [12], the optimal conditions of the PPC mode obtained by using the Taguchi orthogonal arrays can extend the battery lifetime by 100 cycles compared with the CC-CV mode.

B. Pulsed Current-Constant Current (PCCC) Mode

In the Pulsed Current-Constant Current (PCCC) mode, a positive pulsed current is followed by a constant current, as shown in Fig. 1(b). The difference between the PPC mode and PCCC mode is that in the PCCC mode, the current of the rest time is not zero but a constant current. The amplitude of the pulses is A_h, while the amplitude of the current during the rest time is A_l. The capacity utilization of the PCCC mode is 80%-95% compared with the CC-CV mode [19]. The charging speed and the capacity fade of the PCCC mode are similar to that of the CC-CV mode [19].

C. Negative Pulsed Current (NPC) Mode

The Negative Pulsed Current (NPC) mode is also called Reflex current mode. In NPC mode, the positive current is followed by a short negative pulsed current and a relaxation time, as shown in Fig. 1(c). The amplitude of the positive pulses and negative pulses are A_p and A_n, respectively. The duration of the positive pulsed current, negative pulsed current, and relaxation in a period are t_p, t_n, and t_r, respectively. Both the duty cycle of the positive pulses and negative pulses can be obtained by Eq. (1). In [20], the NPC mode can improve the active material utilization to prolong the battery lifetime by 900 cycles. The negative pulses can decrease the growth rate of the ohmic resistance and of the charge transfer resistance with aging; furthermore, the rate of the battery capacity fade can also be decreased when using this current mode [21]. The NPC mode with lower amplitude and frequency improves the charging capacity by around 3.5% compared with that with higher amplitude and frequency [22].

D. Alternating Pulsed Current (APC) Mode

The Alternating Pulsed Current (APC) mode is inserted in the discharging pulses periodically during the constant charging current, as shown in Fig. 1(d). The meaning of each symbol is the same as the NPC mode. In [13], the APC mode with a large range of frequency, current amplitude, and duty cycle was investigated. The results illustrate that the APC mode has no positive effect on the battery charging/discharging performance [13]. In [23], the APC mode at a frequency of 10 kHz can reduce the capacity fade and the maximum rising temperature by around 6.5% and 25%, respectively compared to that at a frequency of 10 Hz.

E. Sinusoidal-Ripple Current (SRC) Mode

The Sinusoidal-Ripple Current (SRC) mode is presented in Fig. 1(e). The amplitude and the offset of SRC are represented by A_{sr} and A_o, respectively. The SRC at different frequencies is investigated and the results shown are similar to the PPC mode in both [16] and [8], although the conclusion of them are different, which has been illustrated in the subsection on the PPC mode. Compared with the CC-CV mode, the SRC can increase the Li-ion battery lifetime by 16.1% [16]. In [25], the SRC mode with the optimal frequency can improve the charging speed and efficiency by 5.1% and 5.6% compared with the CC-CV mode. However, the authors in [17] report that the SRC mode does not affect the charging time but results in an increase in cell temperature compared to the CC mode. Furthermore, the SRC has no significant impact on the capacity fade in the frequency range from 1 Hz to 1 kHz compared to the CC mode [24].

TABLE I
THE EXISTING STUDY ON THE PULSED-CURRENT CHARGING AND THE SINUSOIDAL-RIPPLE-CURRENT CHARGING.
(NMC: $LiNiMnCoO_2$, LIPO: LITHIUM-ION POLYMER, LCO: $LiCoO_2$, LFP: $LiFePO_4$.)

Reference	Chemical system	Current mode	frequency [Hz]	Compared to	Discharging capacity	Charging time	Temperature rise	Lifetime
[16]	NMC	PPC SRC	1-10k	CC-CV	√	√	√	× √
[8]	-	PPC, PPC-CV, SRC, SRC-CV	2k	CC, CC-CV	√	√	√	×
[12]	LiPo	PPC	100-100k	CC-CV	×	×	×	√
[15]	NMC	PPC-CV	50, 100, 1k	CC-CV	×	√	×	√
[19]	NMC, LCO, LFP	PCCC	1, 25	CC-CV	√	√	×	√
[20]	LCO	NPC	-	CC	×	×	×	√
[21], [22]	LFP	NPC-CV	-	CC, CC-CV	×	×	×	√
[13]	LFP	APC	0.2-100	CC-CV	√	×	×	×
[23]	LCO	APC	1-10k	CC-CV	×	×	√	√
[17]	NMC	PPC, SRC	158, 228	CC	×	√	√	×
[24]	NMC	SRC	1, 100, 1k	CC	×	×	×	√
[25]	LFP	SRC	1-600	CC	×	√	√	×
This work	NMC	PPC, PCCC, NPC, APC, SRC, ASRC	1-1k	CC	√	√	√	×

F. Alternating Sinusoidal-Ripple Current (ASRC) Mode

The Alternating Sinusoidal-Ripple Current (ASRC) mode can be regarded as the SRC mode that obtained a dc offset, which allows the battery discharged periodically during the charging process. Corresponding to the PPC mode and APC mode, the ASRC mode is proposed in this work, which is the SRC mode obtained a dc offset, as shown in Fig. 1(f). The meaning of each symbol is the same as in the SRC mode.

G. Summary

The impacts of the current mode on the performance and lifetime of Li-ion batteries are presented to some extent in the available literature. Table I summarizes the existing studies on the different current mode. However, the obtained results are inconclusive because various Li-ion battery chemistries were used in the summarized studies. Moreover, the existing studies have a different way to evaluate the impact on Li-ion battery cells, and each of them is usually only studying one or two charging current modes. The objective of this work is to experimentally investigate and analyze the impact of six current modes at different frequencies on NMC cell performance (i.e., maximum rising temperature, discharging capacity, and charging speed). According to the experimental results, the advantages and disadvantages for each current mode can be summarized, which can be the guidance for designing an advanced charging strategy.

III. EVALUATION CRITERIA FOR BATTERY CHARGING PERFORMANCE

The CC charging mode is selected as the standard to evaluate the considered current modes in this work. To evaluate unbiassed the impact of different current modes on the battery performance, the average current is the same for all current modes. The cylindrical NMC cell HTCNR18650 is used for performing these investigations. The specifications of the cell are summarized in Table II.

TABLE II
SPECIFICATIONS OF THE TESTED NMC CELL.

Parameter	Value
Model	HTCNR18650
Format	Cylindrical cell
Chemical system	NMC
Nominal capacity, Cap_n	2,200 mAh
Nominal voltage, V_n	3.6 V
Charging cut-off voltage, V_{max}	4.2 V
Discharging cut-off voltage, V_{min}	2.5 V
Maximum (dis)charging current, I_{max}	3 C (6.6 A)

A. Maximum Rising Temperature

The battery temperature is determined by the overpotential heat Q_P, the heat due to changes in entropy Q_S, and the transferred heat Q_B; nevertheless, the overpotential heat Q_P is the dominant part, which is responsible for the rising temperature [26]. The overpotential heat Q_P can be calculated as follows:

$$Q_P = I_{rms}^2 Z_{real}(f) \tag{2}$$

where $Z_{real}(f)$ is the real part of the battery impedance. Therefore, the RMS value of the current I_{rms} and the real part of the impedance $Z_{real}(f)$ are the two variables that affect the rising temperature during the charging process. The equivalent circuit model of the battery, presented in Fig. 2, is considered for analyzing the charging process of each current mode. The model is composed of the ohmic resistance R_o, the charge transfer resistance R_p, and the electric double-layer capacitance C_p of the electrode interface. The battery impedance $Z(f)$ can be described, as follows:

$$Z(f) = R_o + \frac{R_p}{1+(2\pi f)^2 R_p^2 C_P^2} - j\frac{2\pi f R_p^2 C_p}{1+(2\pi f)^2 R_p^2 C_P^2} \tag{3}$$

Therefore, $Z_{real}(f)$ can be determined by:

$$Z_{real}(f) = R_o + \frac{R_p}{1+(2\pi f)^2 R_p^2 C_P^2} \tag{4}$$

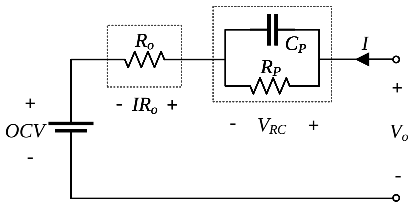

Fig. 2. First-order equivalent circuit model of the Li-ion battery.

The RMS value of each mode can be calculated by follows:

$$I_{rms.CC} = I_{CC} \tag{5}$$

$$I_{rms.PPC} = \sqrt{D_p A_p^2} \tag{6}$$

$$I_{rms.PCCC} = \sqrt{D_p A_h^2 + (1 - D_p) A_l^2} \tag{7}$$

$$I_{rms.NPC} = I_{rms.APC} = \sqrt{D_p A_h^2 + D_n A_l^2} \tag{8}$$

$$I_{rms.SRC} = I_{rms.ASRC} = \sqrt{\frac{1}{2} A_{sr}^2 + A_o^2} \tag{9}$$

The maximum rising temperature ΔT_{max} is the difference between the initial temperature $T_{init.}$ and the maximum temperature $T_{max.}$ of the cell during the charging process:

$$\Delta T_{max} = T_{max.} - T_{init.} \tag{10}$$

The temperature of the battery cell will be measured and monitored during all tests.

B. Discharging Capacity

The battery voltage V_o is the sum of the open-circuit voltage OCV, the voltage drop over the ohmic resistance V_Ω, and the voltage drop over the RC parallel network V_{RC}; all these voltages are dependent on the State-of-Charge (SOC). The SOC can be obtained by the Coulomb counting method:

$$SOC = \frac{1}{3600 \cdot Cap} \int_0^t I dt \cdot 100\% \tag{11}$$

where Cap is the battery capacity and I is the charging current. The ohmic resistance R_o can be measured by the Hybrid Pulse Power Characteristic (HPPC) test [27], [28]. The R_o is the ratio of the voltage changes to current changes and determined with a 5% SOC resolution. There is a 15-minute relaxation period between positive and negative pulses. The average of the charging and discharging ohmic resistance is considered as the cell's R_o at the corresponding SOC. An accurate relationship expression between the R_o and the SOC is given by:

$$R_o = 0.011 \cdot e^{-0.041 \cdot SOC} + 0.0336 \tag{12}$$

The measured and fitted R_o are shown in Fig. 3(a). The battery cell is charged from 0% SOC to 100% SOC. Once the charging capacity reaches 5% of the total battery capacity, the cell is rested for 4 h. Then, the measured terminal voltages are considered as the OCVs of the battery cell. The discharging OCV can be also obtained in this way. The average OCV between the charging and discharging processes is used to form the $OCV - SOC$ characteristic [29]. An accurate relationship expression between the OCV and the SOC is given by:

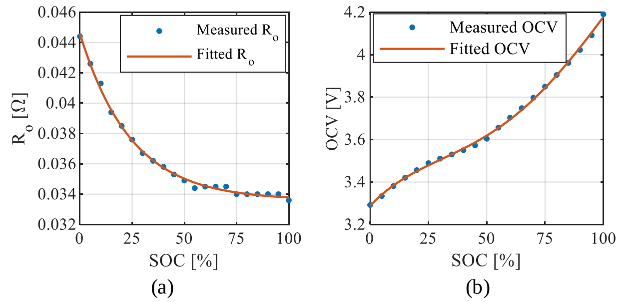

Fig. 3. (a) Measured and fitted R_o versus SOC and (b) measured and fitted OCV versus SOC.

$$\begin{aligned} OCV = &- 1.167 \cdot SOC^4 + 3.178 \cdot SOC^3 \\ &- 2.268 \cdot SOC^2 + 1.145 \cdot SOC^1 + 3.289 \end{aligned} \tag{13}$$

The measured and fitted OCV are shown in Fig. 3(b). Battery terminal voltage V_o can be measured in real-time. The RC voltage V_{RC} can be obtained by follows:

$$V_{RC}(SOC) = V_o - OCV(SOC) - IR_o(SOC) \tag{14}$$

The rising temperature during the charging process mainly influences the charge transfer reaction process, while has no significant effect on the ohmic resistance [30]–[32]. Therefore, the effect of the changes in the cell temperature on the ohmic resistance is ignored in this analysis [33]. Due to the same average current, the changes in $OCV(SOC)$ and $IR(SOC)$ are the same for different current modes. Thus, the V_{RC} has an impact on the charging process, especially when the battery terminal voltage is approaching the charging cut-off voltage V_{max}. If a current mode can decrease the V_{RC}, the $OCV(SOC)$ will have more margin for the voltage rise, which allows the battery to charge more and thus obtain a higher discharging capacity. Moreover, different current modes can affect the charging efficiency. Therefore, the discharging capacity is used to determine the available capacity, which is obtained by applying the same constant discharging current. The improvement of the discharging capacity ΔCap is defined as follows:

$$\Delta Cap[\%] = \frac{Cap_{dis} - Cap_{dis.CC}}{Cap_{dis.CC}} \cdot 100\% \tag{15}$$

where Cap_{dis} is the discharging capacity obtained by the different current mode charging and $Cap_{dis.CC}$ is the discharging capacity obtained by the standard CC mode charging.

C. Charging Speed

The performance of the charging mode can be also reflected by the charging speed α, which is defined in Eq. (16) as the ratio between the available discharging capacity Cap_{dis} (after charging with various current modes) and the pulsed current charging time t_{cha}:

$$\alpha = \frac{Cap_{dis}}{t_{cha}} \tag{16}$$

A higher α value means a faster charging speed of the current mode.

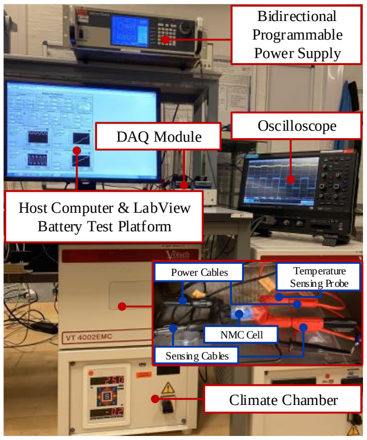

Fig. 4. Experimental platform.

IV. Experiment and Results

A. Experimental Setup

The experimental setup consists of a National Instruments (NI) cDAQ-9172 Data Acquisition (DAQ) module and a KEPCO BOP 100-10 MG bidirectional programmable power supply, as shown in Fig. 4. The analogy output module NI 9263 is used to transfer the reference of the current mode from the host computer to the power supply, while an analogy input module NI 9215 is used to measure the voltage and current of the battery cell. A thermocouple wire was placed on the surface of the cell to measure and monitor its temperature. The temperature is measured by a NI 9122 thermocouple input module. The Battery test platform is developed by LabView to generate the reference of the current modes for the KEPCO and to log the battery cell voltage, current, and temperature. To reduce the impact of the changes in the ambient temperature, the battery cell was placed in a VT 4002EMC climatic chamber that the temperature was set at 25 °C.

B. Experimental Procedures

Ten cases were performed in this work. The conditions of the ten cases are presented in Table III, where Cases 5-7 are the APC mode with different amplitudes or duty cycles, and Cases 9-10 are the ASRC mode with different amplitudes. Four frequencies (i.e., 1 Hz, 10 Hz, 100 Hz, and 1 kHz) are applied in Cases 2-10. Exemplification of the current waveforms for the ten cases is presented in Fig. 5, where the frequency for Cases 2-10 is 1 Hz. The discharging battery capacity for each case is obtained by discharging the battery with a constant current of 0.5 C (i.e., 1.1 A). Before the test, the cell was fully discharged by a 0.5-C constant current and then tempered at 25 °C in the climate chamber for one hour. Each test case consists of the following four steps:

1) Relaxation of the battery cell at 25 °C for one hour.
2) Full charging of the battery cell by applying the studied current modes and the corresponding frequencies until the charging cut-off voltage of 4.2 V is reached.
3) Relaxation of the battery cell at 25 °C for one hour.
4) Full discharging of the battery cell by applying a constant current of 0.5 C until the discharging cut-off voltage of 2.5 V is reached.

TABLE III
Parameters of the Current Mode for Ten Cases.

Current mode		Parameters			
Case 1	CC	1 C			
		$A_p(A_h)$ [C]	$D_p(D_h)$ [%]	$A_n(A_l)$ [C]	$D_n(D_l)$ [%]
Case 2	PPC	2	50	-	-
Case 3	PCCC	1.5	50	0.5	50
Case 4	NPC	2	60	2	10
Case 5	APC	2	75	2	25
Case 6	APC	2.5	50	0.5	50
Case 7	APC	3	50	1	50
		A_{sr} [C]		A_o [C]	
Case 8	SRC	1		1	
Case 9	ASRC	1.5		1	
Case 10	ASRC	2		1	

During the test process, the battery cell was placed in the climate chamber in order to ensure that the cell reaches thermal stability. Step 1 and Step 3 can make sure that the initial temperature of the battery cell for all tests is the same.

C. Experimental Results

The measured voltage and temperature during the charging process are presented, as shown in Fig. 6, where the frequency for Cases 2-10 is 1 Hz. The discharging capacity, the charging time, and the maximum rising temperature of the battery cell charged using different cases are summarized in Table IV, Table V, and Table VI, respectively. In these three tables, colors show the difference in values. The darker the color, the larger the corresponding value. The experimental results obtained when the cell is charged using Case 1 (i.e., CC mode) is regarded as the reference, which is used to evaluate the effect of the other nine cases on the performance of the NMC cell. It is observed that the battery cell charged using the CC mode has the lowest discharging capacity, the shortest charging time, and the lowest rising temperature.

First, the effect of different current modes at a frequency of 1 Hz on the battery performance is analyzed by the experimental results presented in Table IV. The influence, from small to large, of the four pulse current modes on the discharging capacity, is PCCC, PPC, NPC, and APC. Compared to the CC mode, the maximum increase in discharging capacity of these four modes are 1%, 2.1%, 4.5%, and 6.2%, respectively. Therefore, we can conclude that the negative pulse has a positive effect on the discharging capacity. Different conditions of the current modes, such as the amplitude and the duty cycles, will lead to different effects on the performance of the battery. The three APC modes (i.e., Cases 5-7) can increase the discharging capacity by 5.3%, 5.1%, and 6.2%, respectively compared with the CC mode. The sinusoidal-ripple current charging modes also improve the discharging capacity. The SRC mode (i.e., Case 8) can increase the discharging capacity by 1.9% compared to the CC mode. Similar to the pulsed current mode, the sinusoidal-ripple-current charging mode with the negative current (i.e., Case 9 and Case 10) can further improve the discharging capacity by up to 4.9% compared to the CC mode. The pulsed current modes can obtain a higher discharging capacity compared to the sinusoidal-ripple current modes when they have the same positive/negative amplitude.

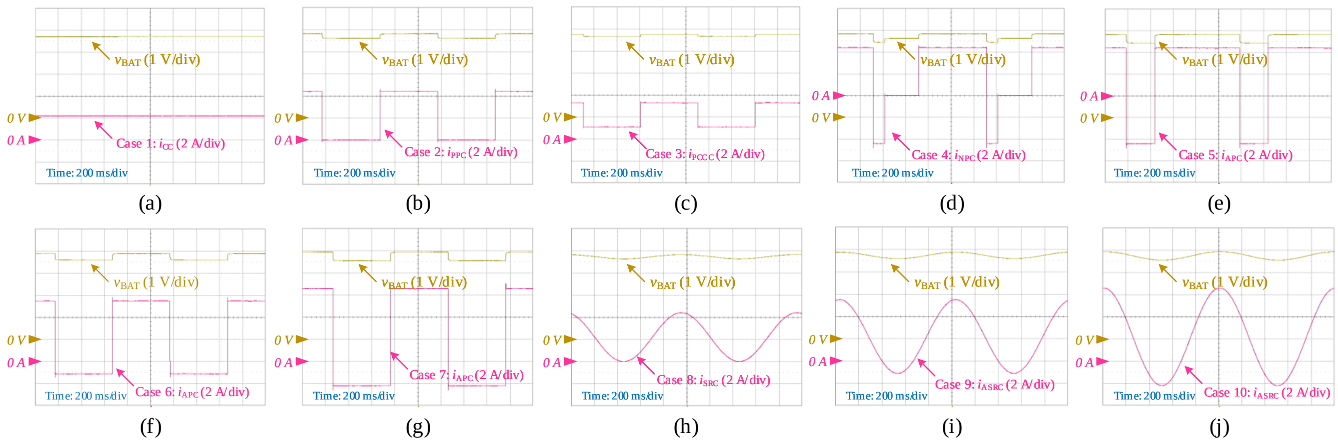

Fig. 5. The waveform of current modes during the experiment: (a) Case 1, (b) Case 2, (c) Case 3, (d) Case 4, (e) Case 5, (f) Case 6, (g) Case 7, (h) Case 8, (i) Case 9, and (j) Case 10; the frequency of Cases 2-10 is 1 Hz.

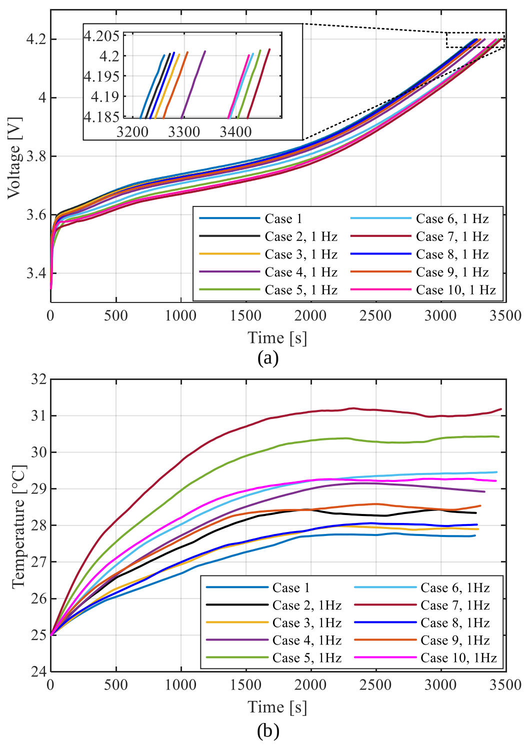

Fig. 6. The battery cell was charged by different current modes with a frequency of 1 Hz at 25 °C ambient temperature: (a) voltage curves and (b) temperature curves.

For example, the discharging capacity of Case 7 (i.e., APC mode) is higher than that of Case 10 (i.e., ASRC mode) by 1.2%, while both the two cases have the same positive and negative amplitude, which are 3 C and 1 C, respectively.

By comparing Table IV and Table V, the charging time is proportional to the discharging capacity, which means that a higher discharging capacity needs a longer charging time.

The maximum rising temperatures, ΔT_{max}, which were measured during all the considered charging modes are summarized in Table VI. When analyzing these results, one should be remembered that different I_{rms} current values were used depending on the charging mode. The highest rising temperature of the battery cell, (i.e., 6.2 °C) is obtained when the battery was charged using Case 7 conditions, where the largest I_{rms} (i.e., $\sqrt{5}I_n \approx 4.92$ A) was used. Contrarily, the lowest rising temperature of the battery cell (i.e., 2.8 °C) is obtained in Case 1, where the smallest I_{rms} (i.e., $I_n = 2.2$ A) was used. Table VII lists the I_{rms} values of the ten charging cases, sorted from small to large. The maximum rising temperature increases with the increase in the I_{rms}.

The frequency of current modes can impact the battery performance. According to the experimental results presented of in Table IV, the current mode at a lower frequency can obtain a higher discharging capacity compared to that of a higher frequency. For Cases 2-9, the current mode at a frequency of 1 Hz can averagely increase the discharging capacity by 0.5% compared to that of 1 kHz. Correspondingly, the charging time of a current mode at a frequency of 1 Hz is averagely longer than that of 1 kHz by 0.5%.

The frequency of the current mode also impacts the temperature during the charging process. According to the shade of color of Table VI, when the battery was charged by the same current mode but at different frequencies, the maximum rising temperature ΔT_{max} of the battery does not change significantly. For all the cases (except Case 1), the changes in ΔT_{max} caused by different sweeping the frequency from 1 Hz to 1 kHz, are below 1 °C. Thus, it can be concluded that for the studied cells, no extra cooling needs to be considered when changing the frequency of the pulsed current charging mode. However, a trend still can be observed, i.e., the maximum rising temperature decreases with the increase in the current frequency. According to Eq. (2), the maximum rising temperature is related to I_{rms} and $Z_{real}(f)$. The I_{rms} is not changed for each current mode as it can be determined by Eqs. (6-9). The real impedance of the battery cell $Z_{real}(f)$ is changed by the frequency for each current mode. An EIS test was performed by using a Digatron battery test station. The battery ac-impedance, which was measured between 6.5 kHz and 10 mHz, is presented in Fig. 7. Both the real impedance $Z_{real}(f)$ and the absolute impedance $|Z(f)|$ of the battery cell decrease as the frequency increases in this frequency range, as shown in Figs. 7(a) and (b), respectively. Therefore, as the frequency of the charging current mode increases, the maximum rising temperature of the battery decreases.

TABLE IV
DISCHARGING CAPACITY OF THE NMC CELL CHARGED BY THE TEN CASES.

Current mode		Cap_{dis} [mAh]			
Case 1	CC	1986			
frequency [Hz]		1	10	100	1k
Case 2	PPC	2027	2022	2019	2016
Case 3	PCCC	2006	2001	2000	1997
Case 4	NPC	2075	2072	2063	2060
Case 5	APC	2092	2090	2088	2085
Case 6	APC	2088	2087	2084	2077
Case 7	APC	2109	2106	2103	2100
Case 8	SRC	2023	2020	2017	2015
Case 9	ASRC	2033	2030	2026	2023
Case 10	ASRC	2084	2082	2078	2075

TABLE V
CHARGING TIME OF THE NMC CELL CHARGED BY THE TEN CASES.

Current mode		t_{cha} [s]			
Case 1	CC	3261			
frequency [Hz]		1	10	100	1k
Case 2	PPC	3273	3265	3260	3255
Case 3	PCCC	3290	3282	3280	3275
Case 4	NPC	3380	3375	3360	3356
Case 5	APC	3447	3443	3440	3435
Case 6	APC	3433	3430	3425	3415
Case 7	APC	3465	3460	3455	3450
Case 8	SRC	3280	3275	3270	3268
Case 9	ASRC	3326	3322	3315	3310
Case 10	ASRC	3425	3421	3415	3410

TABLE VI
MAXIMUM RISING TEMPERATURE OF THE NMC CELL CHARGED BY THE TEN CASES.

Current mode		ΔT_{max} [°C]			
Case 1	CC	2.8			
frequency [Hz]		1	10	100	1k
Case 2	PPC	3.4	3.4	3.4	3.3
Case 3	PCCC	3.0	2.8	2.8	2.7
Case 4	NPC	4.2	4.2	4.0	3.7
Case 5	APC	5.4	5.4	4.9	4.7
Case 6	APC	4.4	4.4	4.4	4.2
Case 7	APC	6.2	5.8	5.6	5.3
Case 8	SRC	3.1	3.0	3.0	2.9
Case 9	ASRC	3.6	3.5	3.5	3.4
Case 10	ASRC	4.3	4.3	4.3	4.0

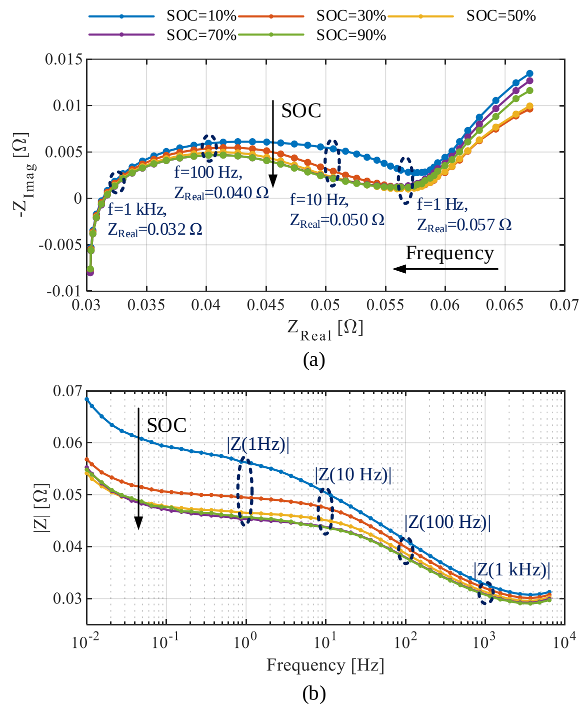

Fig. 7. The ac-impedance spectrum of the tested cell at different SOCs: (a) Nyquist plot and (b) the absolute impedance.

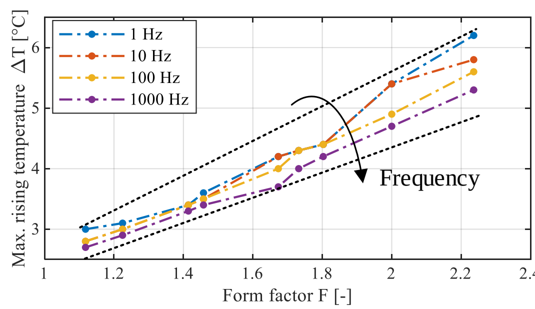

Fig. 8. The maximum rising temperature of various current modes as a function of the form factor and frequency at 25 °C ambient temperature.

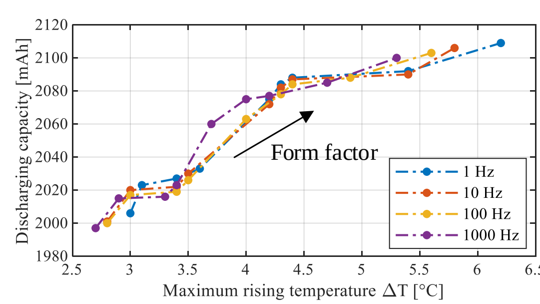

Fig. 9. The discharging capacity vs. the maximum rising temperature.

Due to the same average current for the different current modes, the form factor F is defined as the ratio between the RMS current value I_{rms} and the average current I_{avg}, i.e., $F = I_{rms}/I_{avg}$ [13]. The form factor F can replace the RMS value of the current I_{rms} to analyze the impact on battery rising temperature without considering the real current value. The maximum rising temperature with different frequencies f and form factors F obtained by different current modes are presented in Fig. 8. It is observed that the form factor F has a dominant influence on the battery rising temperature compared to the frequency. This is because the magnitude of the I_{rms} is much greater than the value of the $Z_{real}(f)$. Fig. 9 shows the increase in the discharging capacity with the temperature rise. A higher temperature can lower the impedance of the battery, thus resulting in a lower terminal voltage, which enables the cell to obtain more charge before reaching the charging cut-off voltage V_{max} [32], [34], [35].

TABLE VII
EXPERIMENTAL RESULTS OF TEN CASES (THE FREQUENCY OF CASES 2-10 IS 1 HZ).

Current mode	I_{avg} [A]	I_{rms} [A]	Charging time t_{cha} [min]	Discharging capacity Cap_{dis} [mAh]	Maximum rising temperature ΔT [°C]	Discharging capacity improvement ΔCap [%]	Charging speed α [mAh/min]
CC-CV (1 C)	-	-	82.5	2208	2.9	11.2	26.8
CC (0.5 C)	$0.5I_n$	$0.5I_n$	116.1	2124	1.2	6.9	18.3
CC (Case 1, 1 C)	I_n	I_n	54.4	1986	2.8	-	36.5
PCCC (Case 3, 1 Hz)	I_n	$\sqrt{1.25}I_n$	54.8	2006	3.0	1.0	36.6
SRC (Case 8, 1 Hz)	I_n	$\sqrt{1.5}I_n$	54.7	2023	3.1	1.9	37.0
PPC (Case 2, 1 Hz)	I_n	$\sqrt{2}I_n$	54.5	2027	3.4	2.1	37.2
ASRC (Case 9, 1 Hz)	I_n	$\sqrt{2.125}I_n$	55.4	2052	3.6	3.3	36.7
NPC (Case 4, 1 Hz)	I_n	$\sqrt{2.8}I_n$	56.3	2075	4.2	4.5	36.8
ASRC (Case 10, 1 Hz)	I_n	$\sqrt{3}I_n$	57.1	2084	4.3	4.9	36.5
APC (Case 6, 1 Hz)	I_n	$\sqrt{3.25}I_n$	57.2	2088	4.4	5.1	36.5
APC (Case 5, 1 Hz)	I_n	$2I_n$	57.5	2092	5.4	5.3	36.4
APC (Case 7, 1 Hz)	I_n	$\sqrt{5}I_n$	57.8	2109	6.2	6.2	36.5

The charging speed of ten cases is summarized in Table VII, where the frequency for Cases 2-10 is 1 Hz. The charging speed of Case 2 (i.e., PPC mode) is slightly higher than that of other cases. However, this effect is due to the correspondingly higher average current (i.e., 2.21 A of Case 2 and 2.2 A of other cases) generated by the power supply. Therefore, the current mode has no significant effect on the charging speed of the Li-ion batteries. The experimental results of the battery cell charged by a 0.5-C CC mode and CC-CV mode are also included in Table VII. Compared to the 1-C CC mode (i.e., Case 1), the 0.5-C CC mode can reduce the maximum rising temperature by 1.6 °C and improve the discharging capacity most by 6.9% among all cases, while the charging time is prolonged by 113.4%. Therefore, the charging speed of the 0.5-C CC mode is significantly lower than the 1-C CC mode by 50.1%. The APC mode of Case 7 can improve the discharging capacity by 6.2%, which is only slightly lower (i.e., 0.7%) than that of 0.5-C CC mode but without sacrificing the charging speed. However, the maximum rising temperature obtained by Case 7 is higher than that of 0.5-C CC mode by 5 °C. The CC-CV mode can improve the discharging capacity by 11.2%, which is the highest among all cases. The maximum rising temperature is similar to that of the 1-C CC mode and is lower than other current modes. However, the charging time is prolonged by more than 50% when compared with that of Cases 1-10.

To further analyze the factor that impacts the charging performance of the battery cell, the effects of the different current modes on the maximum rising temperature, discharging capacity, and charging speed are evaluated, as shown in Fig. 10. The evaluation score for each charging performance is obtained by the *normalize* function in MATLAB. The 0.5-C CC mode presents the best performance in rising temperature and discharging capacity, while it has the lowest charging speed due to the low current rate. The charging speed of the considered current modes is the same as the 1-C CC mode. Therefore, the charging speed is defined by the average charging current rate

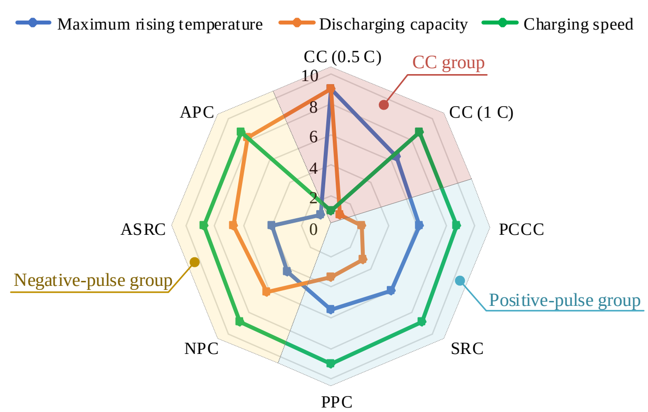

Fig. 10. Effect of different current modes on the charging performance of tested Li-ion batteries.

and not affected by the charging current profiles. However, the rising temperature and discharging capacity are not identical to the different current modes. In Fig. 10, the investigated current modes are categorized into the positive-pulse group and the negative-pulse group according to the charging modes with or without the discharging current during the charging process. The positive-pulse group includes the PCCC mode, SRC mode, and PPC mode. The negative-pulse group includes NPC mode, ASRC mode, and NPC mode. The maximum rising temperature of the positive-pulse group is similar to that of the 1-C CC mode, while the negative-pulse group leads to a higher rising temperature. On the contrary, the negative-pulse group enables the battery cell to obtain a higher discharging capacity than the positive-pulse group. Therefore, the battery charging performance changes resulting from the positive-pulse group are minimal, while that of the negative-pulse group is significant. However, there is not a clear correlation between the rising temperature and the discharging capacity, independent of the current mode. Furthermore, the frequency of these current modes has minimal effect on the battery charging performance according to experimental results. The results obtained by this work are consistent with that of most of the previous studies [8], [15], [17], [25]. Only a few studies show different results with this work, e.g., [16].

V. Conclusion And Future Investigation

This paper investigated four pulsed current charging and two sinusoidal-ripple current charging, which are PPC, PCCC, NPC, APC, SRC, and ASRC, respectively. Furthermore, four frequencies (i.e., 1 Hz, 10 Hz, 100 Hz, and 1 kHz) were considered to study their effect on the maximum rising temperature, discharging capacity, and charging speed. The obtained capacities of the battery cell are slightly different with the various current modes, while the charging speed is the same for all current modes. Thus, the charging speed is determined by the charging current rate and not by the charging current profile. The maximum rising temperature of the battery during the charging process is related to the RMS value of the charging current I_{rms}; a higher I_{rms} of the current mode will increase the battery temperature. For each investigated charging current mode, a lower frequency can obtain the results of a higher discharging capacity, longer charging time, and higher rising temperature. Nonetheless, the changes in the frequency of the current mode have a negligible difference in these battery performances. The charging performance of the PPC mode, SRC mode, and PCCC mode is similar to that of the CC mode. In contrast, the APC mode, NPC mode, and ASRC mode, which includes negative current during the charging process, result in a high rising temperature of the Li-ion batteries.

Future work includes the investigation of the effect of the pulsed current charging mode at different frequencies, amplitudes, and duty cycles on the battery lifetime. Moreover, considering the practical applications, the effect of pulsed current charging mode on the battery pack will be studied in future work.

References

[1] I.-Y. L. Hsieh, M. S. Pan, and W. H. Green, "Transition to electric vehicles in china: Implications for private motorization rate and battery market," *Energy Policy*, vol. 144, p. 111654, Sep. 2020.

[2] N. O. Kapustin and D. A. Grushevenko, "Long-term electric vehicles outlook and their potential impact on electric grid," *Energy Policy*, vol. 137, p. 111103, Feb. 2020.

[3] Q. Lin, J. Wang, R. Xiong, W. Shen, and H. He, "Towards a smarter battery management system: A critical review on optimal charging methods of lithium ion batteries," *Energy*, vol. 183, pp. 220–234, Sep. 2019.

[4] Y. Li, K. Li, Y. Xie, J. Liu, C. Fu, and B. Liu, "Optimized charging of lithium-ion battery for electric vehicles: Adaptive multistage constant current–constant voltage charging strategy," *Renewable Energy*, vol. 146, pp. 2688–2699, Feb. 2020.

[5] Y. Liu, Y. Zhu, and Y. Cui, "Challenges and opportunities towards fast-charging battery materials," *Nature Energy*, vol. 4, no. 7, pp. 540–550, Jun. 2019.

[6] H. Li, X. Zhang, J. Peng, J. He, Z. Huang, and J. Wang, "Cooperative CC–CV charging of supercapacitors using multicharger systems," *IEEE Trans. Ind. Electron.*, vol. 67, no. 12, pp. 10 497–10 508, Dec. 2020.

[7] L. K. Maia, L. Drunert, F. L. Mantia, and E. Zondervan, "Expanding the lifetime of li-ion batteries through optimization of charging profiles," *J. Cleaner Production*, vol. 225, pp. 928–938, Jul. 2019.

[8] S.-Y. Cho, I.-O. Lee, J.-I. Baek, and G.-W. Moon, "Battery impedance analysis considering DC component in sinusoidal ripple-current charging," *IEEE Trans. Ind. Electron*, vol. 63, no. 3, pp. 1561–1573, Mar. 2016.

[9] A. S. Mussa, M. Klett, M. Behm, G. Lindbergh, and R. W. Lindstrom, "Fast-charging to a partial state of charge in lithium-ion batteries: A comparative ageing study," *J. Energy Storage*, vol. 13, pp. 325–333, Oct. 2017.

[10] J. M. Amanor-Boadu, A. Guiseppi-Elie, and E. Sanchez-Sinencio, "Search for optimal pulse charging parameters for li-ion polymer batteries using taguchi orthogonal arrays," *IEEE Trans. Ind. Electron.*, vol. 65, no. 11, pp. 8982–8992, Nov. 2018.

[11] L.-R. Chen, J.-J. Chen, N.-Y. Chu, and G.-Y. Han, "Current-pumped battery charger," *IEEE Trans. Ind. Electron.*, vol. 55, no. 6, pp. 2482–2488, Jun. 2008.

[12] J. Amanor-Boadu, A. Guiseppi-Elie, and E. Sánchez-Sinencio, "The impact of pulse charging parameters on the life cycle of lithium-ion polymer batteries," *Energies*, vol. 11, no. 8, p. 2162, Aug. 2018.

[13] F. Savoye, P. Venet, M. Millet, and J. Groot, "Impact of periodic current pulses on li-ion battery performance," *IEEE Trans. Ind. Electron.*, vol. 59, no. 9, pp. 3481–3488, Sep. 2012.

[14] X. Huang, Y. Li, A. B. Acharya, X. Sui, J. Meng, R. Teodorescu, and D.-I. Stroe, "A review of pulsed current technique for lithium-ion batteries," *Energies*, vol. 13, no. 10, p. 2458, May. 2020.

[15] D. R. R. Kannan and M. H. Weatherspoon, "The effect of pulse charging on commercial lithium nickel cobalt oxide (NMC) cathode lithium-ion batteries," *J. Power Sources*, vol. 479, p. 229085, Dec. 2020.

[16] L.-R. Chen, S.-L. Wu, D.-T. Shieh, and T.-R. Chen, "Sinusoidal-ripple-current charging strategy and optimal charging frequency study for li-ion batteries," *IEEE Trans. Ind. Electron.*, vol. 60, no. 1, pp. 88–97, Jan. 2013.

[17] A. Bessman, R. Soares, S. Vadivelu, O. Wallmark, P. Svens, H. Ekstrom, and G. Lindbergh, "Challenging sinusoidal ripple-current charging of lithium-ion batteries," *IEEE Trans. Ind. Electron.*, vol. 65, no. 6, pp. 4750–4757, Jun. 2018.

[18] X. Huang, Y. Li, J. Meng, X. Sui, R. Teodorescu, and D.-I. Stroe, "The effect of pulsed current on the performance of lithium-ion batteries," in *Proc. IEEE ECCE*, pp. 5633–5640, Oct. 2020.

[19] P. Keil and A. Jossen, "Charging protocols for lithium-ion batteries and their impact on cycle life—an experimental study with different 18650 high-power cells," *J. Energy Storage*, vol. 6, pp. 125–141, May. 2016.

[20] J. Li, E. Murphy, J. Winnick, and P. A. Kohl, "The effects of pulse charging on cycling characteristics of commercial lithium-ion batteries," *J. Power Sources*, vol. 102, no. 1-2, pp. 302–309, Dec. 2001.

[21] M. Abdel-Monem, K. Trad, N. Omar, O. Hegazy, P. V. den Bossche, and J. V. Mierlo, "Influence analysis of static and dynamic fast-charging current profiles on ageing performance of commercial lithium-ion batteries," *Energy*, vol. 120, pp. 179–191, Feb. 2017.

[22] M. A. Monem, K. Trad, N. Omar, O. Hegazy, B. Mantels, G. Mulder, P. V. den Bossche, and J. V. Mierlo, "Lithium-ion batteries: Evaluation study of different charging methodologies based on aging process," *Appl. Energy*, vol. 152, pp. 143–155, Aug. 2015.

[23] M. Uno and K. Tanaka, "Influence of high-frequency charge–discharge cycling induced by cell voltage equalizers on the life performance of lithium-ion cells," *IEEE Trans. Veh. Technol.*, vol. 60, no. 4, pp. 1505–1515, May. 2011.

[24] A. Bessman, R. Soares, O. Wallmark, P. Svens, and G. Lindbergh, "Aging effects of AC harmonics on lithium-ion cells," *J. Energy Storage*, vol. 21, pp. 741–749, Feb. 2019.

[25] Y.-D. Lee and S.-Y. Park, "Electrochemical state-based sinusoidal ripple current charging control," *IEEE Trans. Power Electron.*, vol. 30, no. 8, pp. 4232–4243, Aug. 2015.

[26] K. Onda, T. Ohshima, M. Nakayama, K. Fukuda, and T. Araki, "Thermal behavior of small lithium-ion battery during rapid charge and discharge cycles," *J. Power Sources*, vol. 158, no. 1, pp. 535–542, Jul. 2006.

[27] J. R. Belt, "Battery test manual for plug-in hybrid electric vehicles," Tech. Rep., Sep. 2010.

[28] W. Li, L. Liang, W. Liu, and X. Wu, "State of charge estimation of lithium-ion batteries using a discrete-time nonlinear observer," *IEEE Trans. on Ind. Electron.*, vol. 64, no. 11, pp. 8557–8565, Nov. 2017.

[29] D.-I. Stroe, "Lifetime models for lithium ion batteries used in virtual power plants," in *Department of Energy Technology*. Aalborg University, 2014.

[30] H. Dai, B. Jiang, and X. Wei, "Impedance characterization and modeling of lithium-ion batteries considering the internal temperature gradient," *Energies*, vol. 11, no. 1, p. 220, Jan. 2018.

[31] J. Zhu, Z. Sun, X. Wei, and H. Dai, “A new lithium-ion battery internal temperature on-line estimate method based on electrochemical impedance spectroscopy measurement,” *J. Power Sources*, vol. 274, pp. 990–1004, Jan. 2015.

[32] D. Andre, M. Meiler, K. Steiner, C. Wimmer, T. Soczka-Guth, and D. Sauer, “Characterization of high-power lithium-ion batteries by electrochemical impedance spectroscopy. i. experimental investigation,” *J. Power Sources*, vol. 196, no. 12, pp. 5334–5341, Jun. 2011.

[33] J. Jiang, Q. Liu, C. Zhang, and W. Zhang, “Evaluation of acceptable charging current of power li-ion batteries based on polarization characteristics,” *IEEE Trans. on Ind. Electron.*, vol. 61, no. 12, pp. 6844–6851, Dec. 2014.

[34] J. Zhu, Z. Sun, X. Wei, H. Dai, and W. Gu, “Experimental investigations of an AC pulse heating method for vehicular high power lithium-ion batteries at subzero temperatures,” *J. Power Sources*, vol. 367, pp. 145–157, Nov. 2017.

[35] S. Zhu, C. Hu, Y. Xu, Y. Jin, and J. Shui, “Performance improvement of lithium-ion battery by pulse current,” *J. Energy Chemistry*, vol. 46, pp. 208–214, Jul. 2020.

Xinrong Huang (S’20) received the M.Sc. degree in electrical engineering from Northwestern Polytechnical University (NPU), Xi’an, China, in 2018. She is supported by China Scholarship Council from 2018 to 2021 and currently working toward the Ph.D. degree in lifetime testing and modeling of Lithium-ion batteries at the Department of Energy Technology, Aalborg University, Aalborg, Denmark.

Her research interests include Lithium-ion battery testing and modeling, battery charging strategies, and battery states estimation.

Wenjie Liu (S’18) received the B.Eng. degree in electrical engineering and the M.Sc. degree in power system from the School of Automation, Northwestern Polytechnical University, Xi’an, China, in 2013 and 2016, respectively. He had the Ph.D. degree in electrical engineering from Aalborg University, Aalborg, Denmark, in 2021.

His research interests include power electronics for renewable energy system, grid-connected converters with stability issues, and impedance source converter for photovoltaic applications.

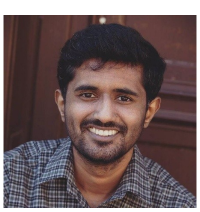

Anirudh Budnar Acharya received B.E (2007) degree in electrical and electronics engineering from VTU, Belgaum, India, MSc (Engg.) (2011) in power electronics from Indian Institute of Science, Bengaluru, India, and Ph.D. (2019) in power electronics from Norwegian University of Science and Technology, Trondheim, Norway. He is a recipient of the Marie Sk?odowska-Curie Actions Individual Fellowship (2018) and is currently a postdoctoral researcher at the Department of Energy, Aalborg University, Aalborg, Denmark. From 2011 to 2015, he was with ABB grid systems R&D as a Scientist wotking on power electronics for the HVDC system.

His research interest include development of power converters for both centralized and distributed renewable energy sources with battery storage solution.

Jinhao Meng (M’19) received the M.S. degree in control theory and control engineering and the Ph.D. degree in electrical engineering from Northwestern Polytechnical University (NPU), Xi’an, China, in 2013 and 2019, respectively. He was supported by the China Scholarship Council as a joint Ph.D. student with the Department of Energy Technology, Aalborg University, Aalborg, Denmark. He is currently an associate researcher in Sichuan University, Chengdu, China.

His research interests include battery modeling, battery states estimation, and energy management of battery energy storage system.

Remus Teodorescu (F’12) received the Dipl.Ing. degree in electrical engineering from the Polytechnical University of Bucharest, Bucharest, Romania, in 1989, and the Ph.D. degree in power electronics from the University of Galati, Galati, Romania, in 1994. In 1998, he joined the Power Electronics Section, Department of Energy Technology, Aalborg University, Aalborg, Denmark, where he is currently a Full Professor. Since 2013, he has been a Visiting Professor with Chalmers University.

His research interests include design and control of grid-connected converters for photovoltaic and wind power systems, high voltage dc/flexible ac transmission systems based on modular multilevel converters, and storage systems based on Li-ion battery technology including modular converters and active battery management systems.

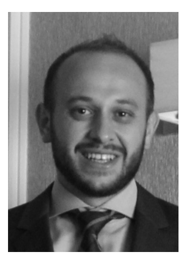

Daniel-Ioan Stroe received the Dipl.-Ing. degree in automatics from ”Transilvania” University of Brasov, Romania, in 2008, and M.Sc. degree in wind power systems from Aalborg University (AAU), Aalborg, Denmark, in 2010. He has been with Aalborg University since 2010, from where he obtained his Ph.D. degree in lifetime modelling of Lithium-ion batteries in 2014. Currently, he is an Associate Professor with AAU Energy, where he leads the Batteries research group and the Battery Systems Testing Lab. He was a Visiting Researcher with RWTH Aachen, Germany, in 2013. He has co-authored over 150 journal and conference papers in various battery-related topics.

His current research interests are in the area of energy storage systems for grid and e-mobility, Lithium-based batteries testing, modelling, diagnostics and their lifetime estimation.